

A novel battery scheme: Coupling nanostructured phosphorus anodes with lithium sulfide cathodes

David Sichen Wu¹, Guangmin Zhou¹, Eryang Mao², Yongming Sun² (✉), Bofei Liu¹, Li Wang³, Jiangyan Wang¹, Feifei Shi¹, and Yi Cui^{1,4} (✉)

¹ Department of Materials Science and Engineering, Stanford University, Stanford, California 94305, USA

² Wuhan National Laboratory for Optoelectronics and School of Optical and Electronic Information, Huazhong University of Science and Technology, Wuhan 430074, China

³ Institute of Nuclear and New Energy Technology, Tsinghua University, Beijing 100084, China

⁴ Stanford Institute for Materials and Energy Sciences, SLAC National Accelerator Laboratory, 2575 Sand Hill Road, Menlo Park, California 94025, USA

© Tsinghua University Press and Springer-Verlag GmbH Germany, part of Springer Nature 2020

Received: 28 October 2019 / Revised: 23 December 2019 / Accepted: 7 January 2020

ABSTRACT

Lithium-ion batteries are approaching their theoretical limit and can no longer keep up with the increasing demands of human society. Lithium-sulfur batteries, with a high theoretical specific energy, are promising candidates for next generation energy storage. However, the use of Li metal in Li-S batteries compromises both safety and performance, enabling dendrite formation and causing fast capacity degradation. Previous studies have probed alternative battery systems to replace the metallic Li in Li-S system, such as a Si/Li₂S couple, with limited success in performance. Recently, there is a focus on red P as a favorable anode material to host Li. Here, we establish a novel battery scheme by utilizing a P/C nanocomposite anode and pairing it with a Li₂S coated carbon nanofiber cathode. We find that red P anode can be compatible in ether-based electrolyte systems and can be successfully coupled to a Li₂S cathode. Our proof of concept full-cell displays remarkable specific capacity, rate and cycling performances. We expect our work will provide a useful alternative system and valuable insight in the quest for next generation energy storage devices.

KEYWORDS

lithium sulfur batteries, red phosphorus, lithium sulfide

1 Introduction

The technological advancement of human civilization has generated an ever-increasing demand for energy storage devices. Conventional lithium-ion batteries, which have served human society for the past decades, are approaching their theoretical limit (~ 420 Wh/kg) [1, 2]. Next generation energy storage systems are urgently needed to satisfy the emerging demands of portable electronics, electric vehicles and renewable energy storage markets. Rechargeable lithium-sulfur (Li-S) batteries, with a high theoretical specific energy of ~ 2,600 Wh/kg, have attracted considerable attention as a promising solution [3–6]. Multiple strategies utilizing nanotechnology and a plethora of hosts/additives have been employed to address the challenges associated with Li-S systems such as poor electrical conductivity, large volume change and dissolution of lithium polysulfide intermediates [7–12].

Despite exciting advances and greatly enhanced performance of Li-S batteries, the use of elemental Li in the system remains a cause of concern. The formation of Li dendrites during cycling can penetrate the separator and lead to short circuit. Additionally, the “hostless” Li metal anode experiences infinite relative volume change during charging and discharging, which will crack the solid electrolyte interphase (SEI) and continuously

consume the active material. Furthermore, Li dendrites greatly increase the surface area and allow the formation of electrochemically inactive “dead Li” [13]. Consequently, Li metal anodes not only generate safety concerns from risk of thermal runaway, but also cause performance issues from rapid capacity decay. As such, despite much ongoing research effort, elemental Li anode has yet to find commercial success in practical rechargeable batteries [14]. One strategy to avoid the problems associated with Li metal while ensuring high energy density is to use a high capacity anode such as silicon, and couple it with a high capacity cathode such as lithium sulfide (Li₂S), the lithiated counterpart of sulfur cathode [15]. This achieved high initial energy densities but suffered significant decay thereafter and exhibited limited cycling capabilities.

Recently, phosphorus (P) has emerged as a very promising candidate anode material due to its high theoretical capacity of 2,595 mAh/g and suitable lithiation potential of 0.7 V [16]. For anode materials, low lithiation potential is desired to achieve high energy density batteries, however, a too low potential (close to 0 V vs. Li⁺/Li) would create safety concerns [17]. Therefore, P is an ideal anode material displaying both high capacity and a relatively low, safe lithiation potential. Of the three allotropes of solid P: White P is chemically unstable and unsuitable for electrode application, black P is difficult to

Address correspondence to Yongming Sun, yongmingsun@hust.edu.cn; Yi Cui, yicui@stanford.edu

synthesize and unfavorable for large-scale production, red P is abundant and environmentally friendly [18]. This makes red P a desirable candidate, however it faces challenges of low conductivity and large volumetric expansion during lithiation. Much progress has been made to address these drawbacks, and red P is usually made into red P-carbon (P/C) nanocomposite structures [19–24]. More recently, remarkable cycling stabilities and fast-charging capabilities of red P anodes have been demonstrated [25].

In this study, we propose a novel nanostructured rechargeable battery enabled by the coupling of red P anode and Li_2S cathode. This is a particularly attractive scheme with high energy density, improved safety and possible long cycling stability. Both red P and S are cheap, abundant and benign to the environment. Li dendrite formation is suppressed by the host materials and the amount of Li needed is reduced in comparison to Li-S systems as there is no longer excess Li in the anode. Such a battery chemistry is efficient, cost effective and suitable for large-scale production on an industrial level.

2 Results and discussion

Figure 1 is a schematic showing the structure of this new P/ Li_2S battery. The anode is comprised of a nanocomposite in which red P partially fills the pores of nanoporous carbon prepared by a vaporization/adsorption strategy. Previous studies have shown that such P/C hybrid structures exhibit high energy densities and stable cycling behavior [26]. The nanoporous carbon serves as a support matrix for the large volume change of phosphorus during the charge/discharge process. In addition, the carbon matrix acts as conductive pathways to the insulating P within the pores. Consequently, the problems associated with the poor electrical conductivity and large volumetric expansion of red P are mitigated. The cathode shown in Fig. 1 consists of a Li_2S coated carbon nanofiber (CNF) membrane. Bulk Li_2S particles face the challenges of poor electrical conductivity, large activation barrier during initial charge and low active-material utilization [27, 28]. A facile liquid infiltration-evaporation coating method is employed to avoid the presence of bulk Li_2S particles. The coated Li_2S experience high utilization and a reduced energy barrier. The CNF matrix acts as a three-dimensional (3D) conductive network enabling fast electron and ion transfer. As a result, the complications that plague Li_2S cathodes are ameliorated.

Enabled by the design in Fig. 1, we will establish the successful coupling of P anodes with Li_2S cathodes to achieve

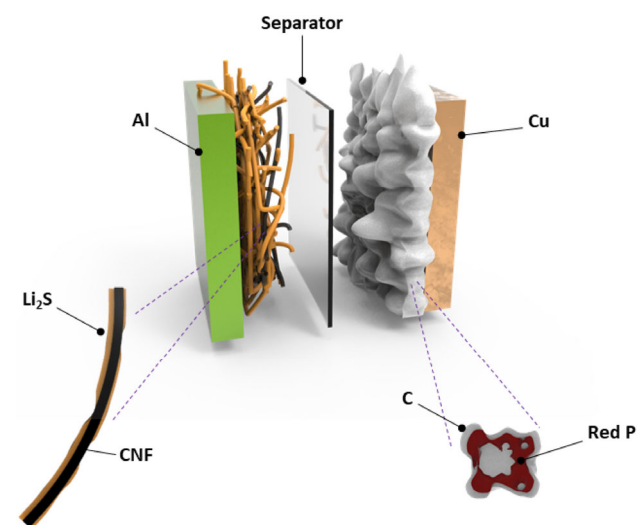


Figure 1 3D schematic of the nanostructured P/ Li_2S battery.

full battery cells with high energy density and long cycling life. Li_2S is the lithiated counterpart of S cathode and acts as a provider of Li-ions in the overall battery chemistry of this P/ Li_2S system. While the alternative of a S cathode and prelithiated red P anode couple (S/ Li_3P) is equally possible, the P/ Li_2S couple is a more expedient and desirable approach from a synthesis perspective. Assuming complete reactions and considering only the active materials, the anode has a theoretical capacity of 2,595 mAh/g, an average potential of ~ 0.7 V (vs. Li^+/Li) and behaves according to the reaction $3\text{Li} + \text{P} \rightarrow \text{Li}_3\text{P}$; the cathode has a theoretical capacity of 1,166 mAh/g, an average potential of ~ 2.2 V (vs. Li^+/Li) and behaves according to the reaction $\text{Li}_2\text{S} \rightarrow 2\text{Li} + \text{S}$. The theoretical specific energy limit of this combination is $\sim 1,200$ Wh/kg, almost three times that of Li-ion batteries. To account for the nanoporous carbon and carbon nanofibers in the design, the practical specific energy limit is ~ 800 Wh/kg for such a P/ Li_2S system.

It must be mentioned that previous reports of red P anodes are primarily based on a carbonate electrolyte system, utilizing combinations of LiPF_6 salt in carbonates such as ethylene carbonate (EC), diethyl carbonate (DEC), dimethyl carbonate (DMC) and ethylene methyl carbonate (EMC) [17–26]. The Li-S system, however, is less compatible with the carbonate electrolyte system and prefers an ether-based system, such as lithium bis(trifluoromethanesulfonyl)imide (LiTFSI) salt in a mixture of dioxolane (DOL) and dimethoxyethane (DME) [3–12]. Therefore, electrolyte compatibility, particularly of red P anode in an ether-based system, must be demonstrated for the P/ Li_2S system to function as desired. Other incompatibility issues and complications, such as unpredictable side reactions, may also arise from this unprecedented system. Therefore, it is imperative to optimize Li/P and Li/ Li_2S half-cells respectively to ensure the performance of the full P/ Li_2S cell.

To fabricate the P/C nanocomposite anode, red P powder and micrometer-scale nanoporous carbon particles are placed separately and sealed in a stainless-steel vessel in pure argon atmosphere. The vessel is heated to 450 °C, just above the sublimation temperature of red P (419 °C), and held for 3 h before gradually cooled to room temperature. This generates P vapors which infiltrate the nanoporous carbon particles and enter the inner nanopores. During the cooling process, the P vapor deposits onto the inner surfaces of the nanopores. Residual P on the P/C nanocomposite particles are washed away using CS_2 solvent. Because solid P has a higher density than P vapor, internal nanoscale void spaces are created and the nanopores of the composite are not fully occupied. This is essential in accommodating the volumetric expansion of P upon lithiation and ensuring long-term cycling performance. The void spaces can act as buffers and restrain the overall expansion of the P/C particles [25]. This promotes the intactness of the particles and the stability of the SEI on the surface. The composition of the P/C nanocomposite is investigated by thermogravimetric analysis (TGA) in a nitrogen atmosphere, and the outcome is shown in Fig. 2(a). The content of phosphorus in the nanoporous carbon is determined to be about 48 wt.%. The contour of the curve infers that there is potentially ~ 33 wt.% of P in micropores and ~ 15 wt.% of P in mesopores. Scanning electron microscopy (SEM) is employed to examine the morphology of the as-prepared P/C nanocomposite. Figure 2(b) shows a secondary electron image of a nanocomposite particle. The P/C nanocomposite has micrometer-scale particles with irregular shapes and a size distribution ranging predominantly from 2 to 10 μm .

To guarantee optimal performance, Li/P half-cells are constructed to evaluate electrodes synthesized through a variety of methods such as hand-mixing, ball-milling and simple

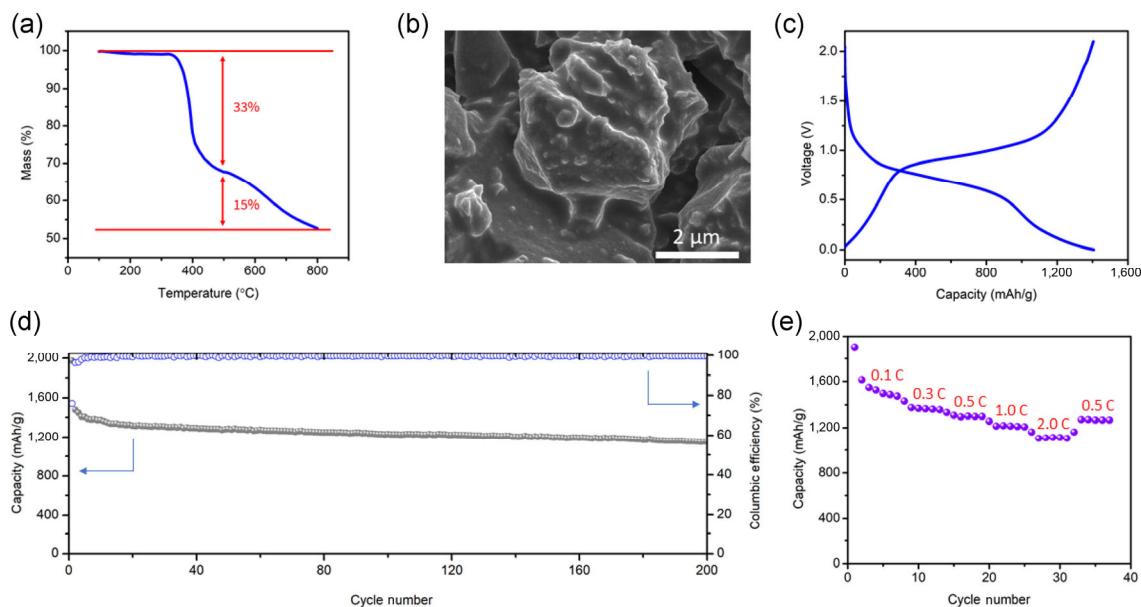


Figure 2 Red P half-cell characterizations. (a) TGA analysis of red P/C nanocomposite. (b) SEM image of red P/C particles. (c)–(e) Red P half-cell electrochemical performance: (c) voltage curves, (d) cycling data and (e) rate capability.

annealing. It is determined that the P/C nanocomposite fabricated by the vapor/adsorption strategy presents far superior initial capacities and capacity retention rates. More importantly, to anticipate compatibility with Li_2S cathode, the conventional carbonate-based electrolyte system for red P anode (1 M LiPF_6 in EC/DMC/EMC 1:1:1 by volume) is juxtaposed with the atypical ether-based electrolyte system for red P anode (1 M LiTFSI in DOL/DME 1:1 by volume). No performance degradations are detected in the ether-based electrolyte system for red P anode compared to the commonly reported carbonate-based electrolyte system. The red P electrode performs equally well under both systems. This exciting finding lays the foundation for the union of red P anode with Li_2S cathode. Furthermore, multiple binder and solvent combinations for red P anode, such as polyvinylidene fluoride (PVDF) + N-methyl-2-pyrrolidone (NMP), polytetrafluoroethylene (PTFE) + ethanol, are rigorously tested and it is established that the combination of carboxymethyl cellulose (CMC) + water offers the best cycling performance, contrary to previous reports that focus on PVDF and PTFE [17–26]. While it may be detrimental for the P/C nanocomposite to be exposed to water, the P within the nanopores of carbon is protected in a short exposure during slurry coating and water is quickly removed thereafter from vacuum drying at 60 °C.

Figure 2(c) depicts the charge/discharge voltage curves during the second cycle of a Li/P half-cell via the as-prepared P/C nanocomposite, cycled between 0–2.1 V (vs. Li^+/Li) with a current density of 0.2 C. The atypical ether-based electrolyte system is used, with CMC + water as binder and solvent. The cell displays typical characteristics of red P, exhibiting stable inclining lithiation and delithiation potential profiles with an average lithiation voltage of ~ 0.7 V (vs. Li^+/Li), delithiation voltage of ~ 1 V (vs. Li^+/Li) and a hysteresis of ~ 0.3 V. A second cycle capacity of 1,420 mAh/g is achieved based on the combined weight of the composite. In accordance to expectation, a large irreversible capacity loss occurs in the first cycle, which can be attributed to the formation of the SEI layer and other possible side reactions consuming the active materials. Figure 2(d) demonstrates the excellent cycling performance of the P/C nanocomposite at 0.5 C in DOL/DME electrolyte. After an initial loss in capacity, the cell rapidly stabilizes and an average Coulombic efficiency of 99.9% is reached. After 100 and 200 cycles, the

cell maintains a reversible capacity of 1,231 and 1,152 mAh/g respectively, corresponding to a retention of 81% from the 2nd cycle to the 200th cycle. The average capacity degradation rate is less than 0.1% per cycle excluding the first cycle. Figure 2(e) illustrates the remarkable rate performance of the P/C nanocomposite under the new aforementioned system. The cell can deliver outstanding capacities of 1,526, 1,368, 1,295, 1,211 and 1,113 mAh/g respectively at the current densities of 0.1 C, 0.3 C, 0.5 C, 1 C and 2 C. Moreover, when the C-rate is adjusted back to 0.5 C from 2 C rates, the capacity recovers to 1,270 mAh/g, a manifestation of the exceptional structural integrity of the P/C nanocomposite.

To fabricate the Li_2S cathode, carbon nanofibers are sonicated in isopropyl alcohol (IPA) to form a dispersion and poured onto a nylon membrane filter. Filtration is performed via a vacuum pump to produce a CNF membrane which is then dried in a vacuum oven. A disc cutter is used to fabricate appropriately sized pieces. Figures 3(a) shows digital photographs of the as-prepared membrane and resultant pieces, respectively. Figure 3(b) is a secondary electron image of the CNF membrane piece examined under SEM, illustrating the 3D network of CNFs which caters a conductive matrix for ion and electron transfer. Li_2S dissolves easily in anhydrous ethanol at elevated temperatures and the dried CNF membrane has high liquid absorption abilities. This favors the application of a facile infiltration-evaporation coating method [27]. A predetermined amount of Li_2S is dissolved in ethanol and dropped onto both sides of these CNF membrane pieces. It should be noted that high purity 200 proof ethanol is required as contaminants within the ethanol can react with Li_2S and severely impair cycling performance. An even distribution of Li_2S throughout the CNF is formulated, and the samples are heated in a glovebox at 260 °C to completely evaporate the ethanol. The Li_2S coated CNF membrane electrode presented is surprisingly facile to construct and can efficiently alleviate the large energy barrier associated with bulk Li_2S particles, improve active material utilization and overall battery performance.

Li/ Li_2S half-cells are assembled to demonstrate the effectiveness of this structure. All cells are initially charged to 4.0 V to facilitate activation of Li_2S . Figure 3(c) depicts the charge/discharge voltage curves during the second cycle of a Li/ Li_2S half-cell via the as-prepared Li_2S electrode, cycled between

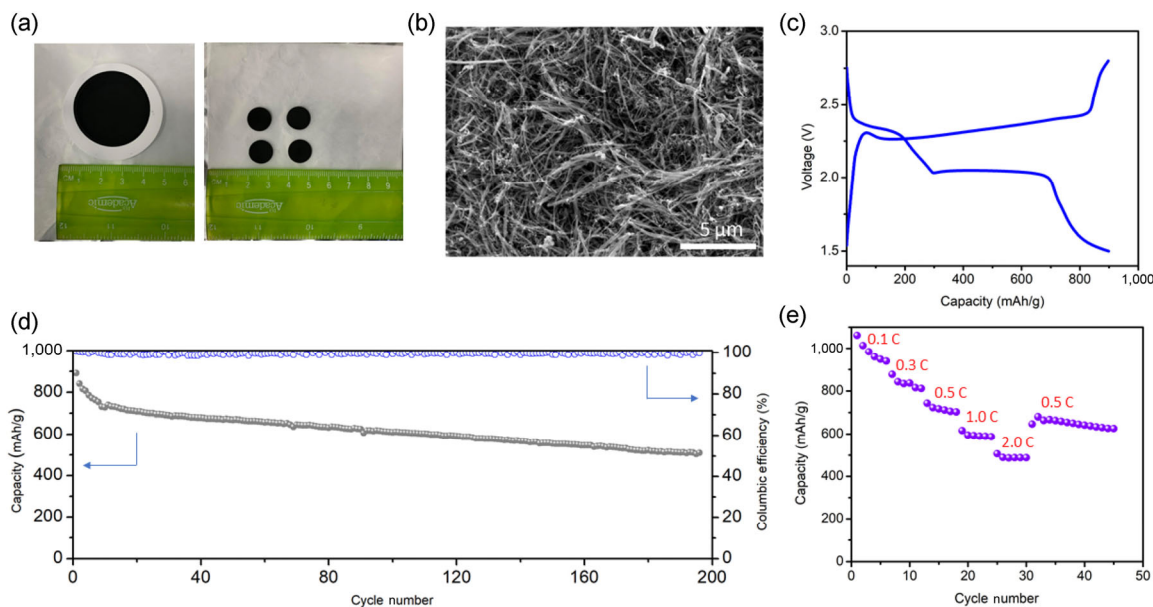


Figure 3 Li_2S half-cell characterizations. (a) Photograph of CNF membranes. (b) SEM image of CNFs. (c)–(e) Li_2S half-cell electrochemical performance: (c) voltage curves, (d) cycling data and (e) rate capability.

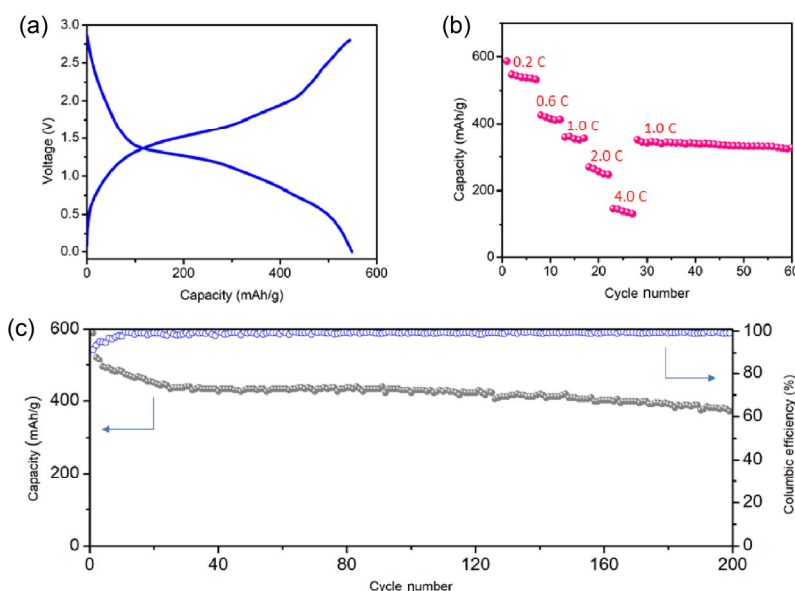


Figure 4 P/ Li_2S full-cell electrochemical performance: (a) voltage curves, (b) rate capability and (c) cycling data.

1.5–2.8 V (vs. Li^+/Li) with a current density of 0.2 C. The cell displays typical characteristics of a Li-S system, with a visible small potential barrier of ~ 0.05 V and a hysteresis of ~ 0.3 V [3–12]. The expected voltage plateaus at ~ 2.3 and ~ 2.0 V are also evident. A second cycle capacity of 895 mAh/g is achieved based on the weight of Li_2S . Figure 3(d) demonstrates the great cycling performance of the Li_2S coated CNF at 0.5 C in DOL/DME electrolyte. An average Coulombic efficiency of 99.8% is reached with gradual capacity loss. After 100 and 200 cycles, the cell maintains a reversible capacity of 610 and 512 mAh/g respectively, corresponding to an average capacity degradation rate of less than 0.2% per cycle. Figure 3(e) illustrates the fine rate performance of the Li_2S electrode. The cell can deliver capacities of 984, 877, 743, 616 and 507 mAh/g respectively at the current densities of 0.1 C, 0.3 C, 0.5 C, 1 C and 2 C. Additionally, when the C-rate is adjusted back to 0.5 C from 2 C rates, the capacity recovers to 680 mAh/g, an indication of the potency of the Li_2S infiltrated CNF structure.

To successfully prove the concept and optimize the full P/ Li_2S cell, the capacities of both electrodes are controlled

and matched. The mass loading of the red P anode and Li_2S cathode is ~ 1.4 and ~ 2.3 mg/cm² respectively, which would produce areal capacity of about ~ 2 mAh/cm². All full-cells are initially charged to 3.6 V to facilitate activation of Li_2S . Figure 4(a) illustrates the charge/discharge voltage curves during the second cycle of a P/ Li_2S full-cell via the capacity matched electrodes, cycled between 0–2.8 V (vs. Li^+/Li) with a current density of 0.2 C. Surveying the individual voltage curves of each of the half-cells as illustrated in Figs. 2(c) and 3(c), the full-cell voltage curve in Fig. 4(a) is in agreement with current theoretical understanding and expectation. The cell exhibits stable inclining potential profiles with an average charging voltage of ~ 1.6 V (vs. Li^+/Li), discharge voltage of ~ 1.2 V (vs. Li^+/Li) and a hysteresis of ~ 0.4 V. A second cycle capacity of 550 mAh/g is obtained via the combined weight of the electrodes.

There are two key points to emphasize. First, the capacity of the full-cell is established on the combined weight of both electrodes (including active and binding materials, excluding current collectors). This is different to the conventional capacity calculations in Li-S battery and red P battery systems, where

the mass of the Li metal in the counter electrode is not accounted for. Therefore, a rough conversion back to the traditional methods reported in Refs. [3–11] would yield 1,100 mAh/g based on the weight of either electrode. Hence the capacity and the energy density of the full-cell is quite remarkable. Second, there is no excess Li in this system. In both Li-S systems and red P anode systems, some Li is consumed in the initial stages due to formation of the SEI and the Li then gradually depletes over longer cycles from factors such as parasitic side reactions, restoration of the SEI and formation of electrochemically inactive “dead Li”. Therefore, the excess Li provided by the Li metal in the counter electrode, often 300% the actual amount needed, is vital to ensuring the outstanding cycling performance commonly reported in Refs. [3–12, 18–28]. In commercial Li-ion batteries, however, this strategy of “excess Li” is no longer applicable and cost effective. The P/Li₂S full-cell presented in this study, in a sense, mimics a commercial Li-ion battery because the capacities of both electrodes are matched, and no excess Li is present in the system other than the standard amount of Li salt in the electrolyte. Consequently, any semblance of long cycle stability becomes even more remarkable and the P/Li₂S has immense potential for future industrialization.

Figure 4(b) demonstrates the long cycling performance of the full P/Li₂S cell at 0.5 C in DOL/DME electrolyte. An average Coulombic efficiency of 99.8% is reached with gradual capacity loss. At 100 and 200 cycles, the cell maintains a reversible capacity of 429 and 378 mAh/g respectively based on the combined weight of the electrodes. This corresponds to an average capacity degradation rate of less than 0.15% per cycle and a retention rate of 72% after 200 cycles. Figure 4(c) illustrates the strong rate performance of the P/Li₂S full-cell. The cell can deliver capacities of 550, 415, 353, 264 and 148 mAh/g respectively at the current densities of 0.2 C, 0.6 C, 1 C, 2 C and 4 C. Furthermore, when the C-rate is adjusted back to 1 C from 4 C rates, the capacity recovers to 343 mAh/g, an implication of the competence of this P/Li₂S full-cell scheme.

This P/Li₂S system is a promising future candidate to address the urgent demand for more efficient energy storage devices in human society. Although the energy density of this novel battery scheme is inferior to that of Li-S batteries, it presents a viable and perhaps more practical alternative with distinct advantages when compared to the Li-S system. 1) The P/Li₂S system does not use bare metallic Li; it improves safety via the elevated potential and suppresses Li dendrite growth via the red P anode host. 2) The P/Li₂S system does not utilize excess Li to boost performance; the capacity of both electrodes is matched; this is compatible with industrial standards for large scale production. 3) The facile fabrication process of both electrodes, the reduced dependence on Li metal and the abundance and low cost of S and red P, all induce this system to be immensely attractive from a commercial perspective.

3 Conclusion

In summary, we successfully demonstrated a novel P/Li₂S battery scheme. Our study indicates that red P anode can be compatible in an ether-based electrolyte system and can be successfully coupled to a Li₂S cathode. Via a facile fabrication process and optimization of both half-cells, our proof of concept full-cell displayed high specific capacity, strong rate capability and compelling cycling performance. While the mass loading and long-term stability of this system can be enhanced, the findings in this study present a useful alternative to those commonly discussed in literature and can inspire additional

investigations. Probes into the mechanisms of the P/Li₂S couple, detailed characterizations of the scheme and inspections of related combinations such as prelithiated P anode and lithium polysulfide cathode may be paramount in perfecting this system. These explorations can provide much needed insight toward achieving superior rechargeable batteries that can eventually replace Li-ion batteries.

Acknowledgements

Y. C. acknowledges the support from the Assistant Secretary for Energy Efficiency and Renewable Energy, Office of Vehicle Technologies of the U.S. Department of Energy, under the Battery Materials Research program and the Battery 500 Consortium program.

Electronic Supplementary Material: Supplementary material (experimental details and supporting figures) is available in the online version of this article at <https://doi.org/10.1007/s12274-020-2645-8>.

References

- [1] Chu, S.; Cui, Y.; Liu, N. The path towards sustainable energy. *Nat. Mater.* **2017**, *16*, 16–22.
- [2] Choi, J. W.; Aurbach, D. Promise and reality of post-lithium-ion batteries with high energy densities. *Nat. Rev. Mater.* **2016**, *1*, 16013.
- [3] Manthiram, A.; Chung, S. H.; Zu, C. X. Lithium–sulfur batteries: Progress and prospects. *Adv. Mater.* **2015**, *27*, 1980–2006.
- [4] Nazar, L. F.; Cuisinier, M.; Pang, Q. Lithium-sulfur batteries. *MRS Bulletin* **2014**, *39*, 436–442.
- [5] Seh, Z. W.; Sun, Y. M.; Zhang, Q. F.; Cui, Y. Designing high-energy lithium–sulfur batteries. *Chem. Soc. Rev.* **2016**, *45*, 5605–5634.
- [6] Ji, X. L.; Nazar, L. F. Advances in Li–S batteries. *J. Mater. Chem.* **2010**, *20*, 9821–9826.
- [7] Wu, D. S.; Shi, F. F.; Zhou, G. M.; Zu, C. X.; Liu, C.; Liu, K.; Liu, Y. Y.; Wang, J. Y.; Peng, Y. C.; Cui, Y. Quantitative investigation of polysulfide adsorption capability of candidate materials for Li-S batteries. *Energy Storage Mater.* **2018**, *13*, 241–246.
- [8] Zhou, G. M.; Tian, H. Z.; Jin, Y.; Tao, X. Y.; Liu, B. F.; Zhang, R. F.; Seh, Z. W.; Zhuo, D.; Liu, Y. Y.; Sun, J. et al. Catalytic oxidation of Li₂S on the surface of metal sulfides for Li–S batteries. *Proc. Natl Acad Sci USA* **2017**, *114*, 840–845.
- [9] Manthiram, A.; Fu, Y. Z.; Chung, S. H.; Zu, C. X.; Su, Y. S. Rechargeable lithium-sulfur batteries. *Chem. Rev.* **2014**, *114*, 11751–11787.
- [10] Yang, Y.; Zheng, G. Y.; Cui, Y. Nanostructured sulfur cathodes. *Chem. Soc. Rev.* **2013**, *42*, 3018–3032.
- [11] Su, D. W.; Zhou, D.; Wang, C. Y.; Wang, G. X. Toward high performance lithium–sulfur batteries based on Li₂S cathodes and beyond: Status, challenges, and perspectives. *Adv. Funct. Mater.* **2018**, *28*, 1800154.
- [12] Kong, L.; Peng, H. J.; Huang, J. Q.; Zhang, Q. Review of nano-structured current collectors in lithium–sulfur batteries. *Nano Res.* **2017**, *10*, 4027–4054.
- [13] Wang, H. S.; Lin, D. C.; Xie, J.; Liu, Y. Y.; Chen, H.; Li, Y. B.; Xu, J. W.; Zhou, G. M.; Zhang, Z. W.; Pei, A. et al. An interconnected channel-like framework as host for lithium metal composite anodes. *Adv. Energy Mater.* **2019**, *9*, 1802720.
- [14] Nishikawa, K.; Fukunaka, Y.; Sakka, T.; Ogata, Y. H.; Selman, J. R. Measurement of concentration profiles during electrodeposition of Li metal from LiPF₆-PC electrolyte solution: The role of SEI dynamics. *J. Electrochem. Soc.* **2007**, *154*, A943–A948.
- [15] Yang, Y.; McDowell, M. T.; Jackson, A.; Cha, J. J.; Hong, S. S.; Cui, Y. New nanostructured Li₂S/silicon rechargeable battery with high specific energy. *Nano Lett.* **2010**, *10*, 1486–1491.
- [16] Wang, Y. L.; Tian, L. Y.; Yao, Z. H.; Li, F.; Li, S.; Ye, S. H. Enhanced reversibility of red phosphorus/active carbon composite as anode for lithium ion batteries. *Electrochim. Acta* **2015**, *163*, 71–76.

- [17] Aurbach, D.; Talyosef, Y.; Markovsky, B.; Markevich, E.; Zinigrad, E.; Asraf, L.; Gnanaraj, J. S.; Kim, H. J. Design of electrolyte solutions for Li and Li-ion batteries: A review. *Electrochim. Acta* **2004**, *50*, 247–254.
- [18] Sun, L.; Zhang, Y.; Zhang, D. Y.; Liu, J. G.; Zhang, Y. H. Amorphous red phosphorus anchored on carbon nanotubes as high performance electrodes for lithium ion batteries. *Nano Res.* **2018**, *11*, 2733–2745.
- [19] Li, W. H.; Yang, Z. Z.; Jiang, Y.; Yu, Z. R.; Gu, L.; Yu, Y. Crystalline red phosphorus incorporated with porous carbon nanofibers as flexible electrode for high performance lithium-ion batteries. *Carbon* **2014**, *78*, 455–462.
- [20] Bai, A. J.; Wang, L.; Li, J. Y.; He, X. M.; Wang, J. X.; Wang, J. L. Composite of graphite/phosphorus as anode for lithium-ion batteries. *J. Power Sources* **2015**, *289*, 100–104.
- [21] Qian, J. F.; Qiao, D.; Ai, X. P.; Cao, Y. L.; Yang, H. X. Reversible 3-Li storage reactions of amorphous phosphorus as high capacity and cycling-stable anodes for Li-ion batteries. *Chem. Commun.* **2012**, *48*, 8931–8933.
- [22] Li, J. Y.; Wang, L.; Ren, Y. M.; Zhang, Y.; Wang, Y. F.; Hu, A. G.; He, X. M. Distinctive slit-shaped porous carbon encapsulating phosphorus as a promising anode material for lithium batteries. *Ionics* **2016**, *22*, 167–172.
- [23] Wang, L. Y.; Guo, H. L.; Wang, W.; Teng, K. Y.; Xu, Z. W.; Chen, C.; Li, C. Y.; Yang, C. Y.; Hu, C. S. Preparation of sandwich-like phosphorus/reduced graphene oxide composites as anode materials for lithium-ion batteries. *Electrochim. Acta* **2016**, *211*, 499–506.
- [24] Qin, X. Y.; Yan, B. Y.; Yu, J.; Jin, J.; Tao, Y.; Mu, C.; Wang, S. C.; Xue, H. G.; Pang, H. Phosphorus-based materials for high-performance rechargeable batteries. *Inorg. Chem. Front.* **2017**, *4*, 1424–1444.
- [25] Sun, Y. M.; Wang, L.; Li, Y. B.; Li, Y. Z.; Lee, H. R.; Pei, A.; He, X. M.; Cui, Y. Design of red phosphorus nanostructured electrode for fast-charging lithium-ion batteries with high energy density. *Joule* **2019**, *3*, 1080–1093.
- [26] Wang, L.; He, X. M.; Li, J. J.; Sun, W. T.; Gao, J.; Guo, J. W.; Jiang, C. Y. Nano-structured phosphorus composite as high-capacity anode materials for lithium batteries. *Angew. Chem.* **2012**, *124*, 9168–9171.
- [27] Zhou, G. M.; Paek, E.; Hwang, G. S.; Manthiram, A. High-performance lithium-sulfur batteries with a self-supported, 3D Li₂S-doped graphene aerogel cathodes. *Adv. Energy Mater.* **2016**, *6*, 1501355.
- [28] Zhou, G. M.; Sun, J.; Jin, Y.; Chen, W.; Zu, C. X.; Zhang, R. F.; Qiu, Y. C.; Zhao, J.; Zhuo, D.; Liu, Y. Y. et al. Sulfophilic nickel phosphosulfide enabled Li₂S impregnation in 3D graphene cages for Li–S batteries. *Adv. Mater.* **2017**, *29*, 1603366.